Microchimica Acta (2021) 188: 89
https://doi.org/10.1007/s00604-021-04747-8

ORIGINAL PAPER

Ratiometric determination of Cr(VI) based on a dual-emission fluorescent nanoprobe using carbon quantum dots and a smartphone app

Chixuan Yao[1] · Qingrun Liu[1] · Ning Zhao[2] · Jing-Min Liu[2] · Guozhen Fang[1] · Shuo Wang[1,2]

Received: 18 November 2020 / Accepted: 3 February 2021 / Published online: 16 February 2021

Abstract

A simple dual-colour fluorescent nanoprobe has been designed composed of blue and yellow emission carbon quantum dots (CQDs). This system is inexpensive and easy to operate and was successfully employed for on-site measurements based on a smartphone app. The designed nanoprobe exhibited increased selectivity for Cr(VI), leading to a double stable response of the two CQDs. The dual-emission nanoprobe showed blue-violet fluorescence upon UV irradiation, and the fluorescent emission peaks were located at 418 nm and 552 nm. The blue light emission of CQDs was quenched with increasing Cr(VI) concentration due to the inner filter effect, whereas the yellow light emission was enhanced due to the aggregation-induced emission effect. The different responses of the dual emissions to Cr(VI) resulted in a fluorescent colour variation, thus enabling facile macroscopic visualization. With a smartphone, the change in the fluorescence colour could be observed more apparently than that of a single fluorescence nanoprobe, and the response increased linearly so that the nanoprobe could be applied to instantaneous measurements. Furthermore, the dual-emission nanoprobe was successfully employed for analysing food and water samples. Accurate concentrations were obtained by constructing a calibration plot using a fluorescence spectrometer and a smartphone app; the recoveries were 81.6% to 107.7%, and the relative standard deviation was below 3.6%. Therefore, this smartphone-integrated dual-emission detection system is promising as a new portable method for the on-site measurement of Cr(VI) ions.

Keywords Fluorescent nanoprobe · Carbon quantum dots · Ratiometric fluorenscence measurement · Visualization detection · Smartphone app · Chromium (VI)

Introduction

Ratiometric fluorescent measurements are primarily performed by measuring the ratios of emission intensity changes at two different fluorescence emission peaks, and this detection method is increasingly used in the food, environmental protection and health care industries [1–3]. Due to the presence of internal standards, ratiometric methods have a built-in correction for environmental disturbance effects while avoiding excitation light intensity fluctuations [4–6] so that the fluorescence intensities of ratiometric nanoprobes are not affected by uncontrollable experimental conditions such as the matrix background and instrument efficiency. Ratiometric fluorescence detection of heavy metal ions has attracted much attention [7, 8]. The frequently used sensing strategies of ratiometric detection are generally based on fluorescence quenching or enhancement, such as inner filter effect (IFE), fluorescence resonance energy transfer (FRET) and aggregation-induced emission effect (AIEE).

Hexavalent chromium, Cr(VI), is one of the main naturally occurring states of chromium [9]. Cr(VI) commonly exists in a variety of modern industries. Cr(VI) is a deleterious environmental contaminant as a result of its allergenicity and carcinogenicity [10]. Thus, it is significant to design a sensor for the rapid, simple and selective determination of Cr(VI). Carbon quantum dots (CQDs) have gained attention as a new type of fluorescent probe due to their distinctive properties. They have the advantages of inexpensive raw material sources, simple

✉ Jing-Min Liu
liujingmin@nankai.edu.cn

✉ Shuo Wang
wangshuo@nankai.edu.cn

[1] State Key Laboratory of Food Nutrition and Safety, Tianjin University of Science & Technology, Tianjin 300457, China

[2] Tianjin Key Laboratory of Food Science and Health, School of Medicine, Nankai University, Tianjin 300071, China

synthesis, good water solubility and biocompatibility, and ultrasmall size [11, 12]. Some ratiometric fluorescence probes using CQDs have been reported in recent years. However, most of them depend on the use of heterologous luminescent materials, so they deserve to be further explored [13–15]. The preparation of these ratiometric fluorescence nanoprobes is an intricate procedure, and the testing process is time-consuming. Therefore, the design of a simple ratiometric nanoprobe equipped with favourable optical characteristics is urgently needed for actual field tests.

In the present research, we prepared two kinds of CQDs: blue emission CQDs (B-CQDs) and yellow emission CQDs (Y-CQDs) to construct a self-assembling fluorescent nanoprobe (named B/Y-CQDs) with different emission peaks, and the obvious change in fluorescence colour could be captured by the naked eye. The nanoscale detection process is controllable and reversible and can be used to determine the fluorescent characteristics of IFE and AIEE processes. In particular, this ratiometric nanoprobe can be successfully applied to detect Cr(VI) using smartphones for instant detection. The RGB colour mode is a colour standard in modern industry. Various colours can be obtained by changing the red (R), green (G) and blue (B) channels and by the superimposition of these channels. This range includes nearly all the colours that the human eye can perceive, making RGB one of the most widely used colour systems. Smartphone-assisted visual results more easily capture small changes in RGB values and are more accurate than the naked eye, and the results show high selectivity, sensitivity and anti-jamming properties.

Materials and methods

Materials and chemicals

All materials and chemicals could be used without purification. O-phenylenediamine, citric acid monohydrate and L-reduced glutathione were obtained from Shanghai Aladdin Bio-Chem Technology Co., Ltd. (https://www.aladdin-e.com/). The interferent metal ions were obtained from Beijing Putiantongchuang Biotechnology Co., Ltd. (http://www.pttc-gbw.com/). Other interferent analytes were obtained from Shanghai Aladdin Bio-Chem Technology Co., Ltd. (https://www.aladdin-e.com/). DI water was used for all solution preparations in this work. In the analysis of possible interferents, all the reagents used were of analytical grade purity.

The synthesis process of CQDs

CQDs were synthesized according to previous works [16, 17]. The described syntheses procedures (in adequate detail) are in the Electronic Supporting Material (ESM).

Characterization

The sizes and morphologies of the B-CQDs, Y-CQDs and B/Y-CQDs were obtained by transmission electron microscopy (TEM) using a FETEM-2100 transmission electron microscope (Japan Electronics Co., Ltd). The fluorescence spectra and the RGB values of B-CQDs, Y-CQDs and B/Y-CQDs were obtained using a fluorescence spectrophotometer F-7100 (Hitachi, Ltd., Japan HQ) and a smartphone app with colour recognition capability. An ultraviolet lamp (Shanghai Precision and Scientific Instrument Corporation, WFH-204b) was applied to obtain fluorescent images of B-CQDs, Y-CQDs and B/Y-CQDs. The particle size was measured by a Mastersizer 3000 (Malvern Panalytical Ltd.). The photoluminescence quantum yield (Φ_f) and the decay curves of the lifetime of CQDs were measured according to previous reports [18, 19].

Construction and characterization of dual-colour fluorescent nanoprobes

The prepared B-CQDs and Y-CQDs were diluted to create solution concentrations of 22.6 μg L^{-1} and 43.2 μg L^{-1}, respectively. Then, Y-CQDs and B-CQDs were mixed at different volume ratios (B-CQDs:Y-CQDs = 2:1, 1:2, 1:4, 1:6, 1:8, 1:10) to optimize the detection conditions. According to the fluorescence colour and fluorescence spectra, the optimal mixing ratio was selected, and then the ratiometric fluorescence probe was constructed using this ratio. According to the sample preparation instructions for different instruments, Y-CQDs, B-CQDs and the ratiometric fluorescence nanoprobe B/Y-CQDs were pretreated to display the structure and optical properties of the material.

Detection of Cr(VI) using the dual-colour fluorescent nanoprobe B/Y-CQDs

B/Y-CQDs exhibited two emission peaks at 418 nm and 552 nm under a single excitation (excitation wavelength (λ_{ex}) was 375 nm), in which the peak at 418 nm represented the emission of B-CQDs and the emission peak at 552 nm represented the emission of Y-CQDs. The optimal mixing ratio for B- and Y-CQDs was 1:6. For Cr(VI) measurement, different levels of Cr(VI) (0–1667 μM) were added to polychromatic fluorescent nanoprobes (B/Y-CQDs) and mixed thoroughly. After 10 min of incubation, the emission fluorescence spectra were recorded at 375 nm for the qualitative and quantitative analyses of Cr(VI). For visual inspection, the sample images and their RGB values were collected by a smartphone under irradiation by a handheld ultraviolet lamp (λ_{ex} = 365 nm, which is common for commercially available UV lamps). For the specific detection method, analogous analytes were mixed with the B/Y-CQDs under the same

detection conditions. Each detection process was repeated three times and performed at room temperature to guarantee the reliability and stability of the empirical data.

Practical applications of B/Y-CQDs

To verify the applicability of the B/Y-CQDs in sample measurement, the fluorescence intensities of the actual samples were recorded at dual-emission peaks of 418 nm and 552 nm, where the excitation wavelength was 375 nm. We chose tap water as the water sample and milk and commercially available green tea as the food samples to illustrate the applicability of the B/Y-CQDs. Before starting the determination, all the determinands needed centrifugation, and then they were passed through a filter membrane (0.45 μm) to remove interfering impurities. Owing to the lack of Cr(VI) in tap water, green tea and in milk, the 250 μL B/Y-CQDs was fortified with 250 μL of various concentrations of Cr(VI) solutions by using the standard addition method. For the food samples, 1 mL of milk sample was added to trichloroacetic acid (9 mL, 9% (*w*/*v*)) under stirring and ultrasound. Then, the mixture was centrifuged to separate proteins, and the pH was adjusted to 7. The relative standard deviation (RSD) was obtained by repeating the process three times under the same experimental conditions.

Results and discussion

Principle of the method

The dual-emission fluorescent B/Y-CQDs composed of B-CQDs and Y-CQDs can be used as an identifying element in heavy metal ion monitoring with dual-colour fluorescence. The construction of dual-emission fluorescent B/Y-CQDs and the operating principle for visual sensing of Cr(VI) are shown in Scheme 1. The B-CQDs and Y-CQDs were prepared based on previous reports [16, 17]. Then, two types of CQDs were mixed in a certain proportion to fabricate the assembled B/Y-CQDs. The fluorescence spectrum of the B/Y-CQDs exhibited dual emission, which was a blend of the original emission of the two CQDs. The mixing of B- and Y-CQDs at a volume ratio of 1:6 resulted in blue-mauve fluorescence. For this reason, the extent of the colour change was described as "violet - yellow", as shown in Scheme 1, and the obtained B/Y-CQDs can be used for the assessment of Cr(VI). The yellow fluorescence of Y-CQDs was enhanced, and the blue fluorescence of B-CQDs was quenched in the presence of Cr(VI). Additionally, the colorimetric fluorescent signals can be conveniently observed by the naked eye. The smartphone app could help to distinguish the intricate changes in fluorescent colours. Most notably, qualitative analysis of Cr(VI) can be achieved via the fluorescent colour variation in the B/Y-CQDs when Cr(VI) is present in actual samples. This colorimetric fluorescent sensing method has the favourable properties of easy operation and low cost, and the smartphone app can take a picture of the samples under UV light (λ_{ex} = 365 nm) to directly monitor its visual signals, making it more sensitive than the naked eye. Therefore, the proposed dual-colour fluorescent B/Y-CQDs could be a rapid and convenient sensor for detecting the heavy metal ion Cr(VI).

Characterizations of B-CQDs, Y-CQDs and the dual-colour fluorescent B/Y-CQDs

Transmission electron microscopy (TEM) was used to determine the morphologies of Y-CQDs and B-CQDs. As Fig. 1a, c shows, it is possible to observe that the two kinds of CQDs have aspherical particles, as reported in other studies. In addition, the histograms of the particle size scattering for CQDs are displayed in Fig. 1b, d, in which it can be verified that the mean sizes of Y-CQDs and B-CQDs are 2.19 and 3.05 nm (the numbers of particles are 100), with particle sizes ranging from 0.88 to 4.25 nm and from 0.72 to 4.82 nm, respectively. The high-resolution TEM images in the illustration reveal that both CQDs have crystalline lattices.

The functional groups in Y-CQDs and B-CQDs were determined by Fourier transform infrared (FTIR) spectroscopy (Fig. 2a). The FTIR spectrum of Y-CQDs shows the stretching vibrations of O-H and N-H (3435 cm^{-1}, 3307 cm^{-1}, 3270 cm^{-1}), C=N or C=O, C=C, and C-O-C (1641 cm^{-1}, 1493.5 cm^{-1}, 1129 cm^{-1}) groups [20, 21]. The FTIR spectrum of B-CQDs showed a wide band in the range of 2200–3700 cm^{-1}, demonstrating the stretching of the N-H of amino groups and the O-H of carboxyl groups in B-CQDs [22]. Three bands (1719, 1403.5 and 1224 cm^{-1}) were attributed to C=O, C-O and O-H in the abundant carboxyl groups of B-CQDs. The peaks at 1129 and 619 cm^{-1} were attributed to the C-N and -NH_2 (which are in aminocarbonyl moieties) group stretching frequencies. The presence of polar functional groups in CQDs allows them to be well dispersed in aqueous solution and facilitates their coordination with Cr(VI) [23]. X-ray photoelectron spectroscopy (XPS) was used to further confirm the constituent elements of the CQDs and is discussed in the ESM. The ultraviolet absorption spectrum shows the optical properties of the nanoprobe. Figure 2b shows the ultraviolet absorption spectra of B-CQDs, Y-CQDs and B/Y-CQDs. The B-CQDs and Y-CQDs both exhibited intense absorbance in the ultraviolet region to the visible light region. The positions of the UV absorption peaks for B-CQDs and Y-CQDs were homologous with the absorption spectra of the CQDs reported previously [16, 17]. The UV-vis spectra of Y-CQDs and B-CQDs have a knee located at 285 nm, and Y-CQDs have an apparent adsorption band centred at 418 nm that was attributed to the π-π* transition of the carbon-carbon double bond [24, 25]. The absorption band at 349 nm was

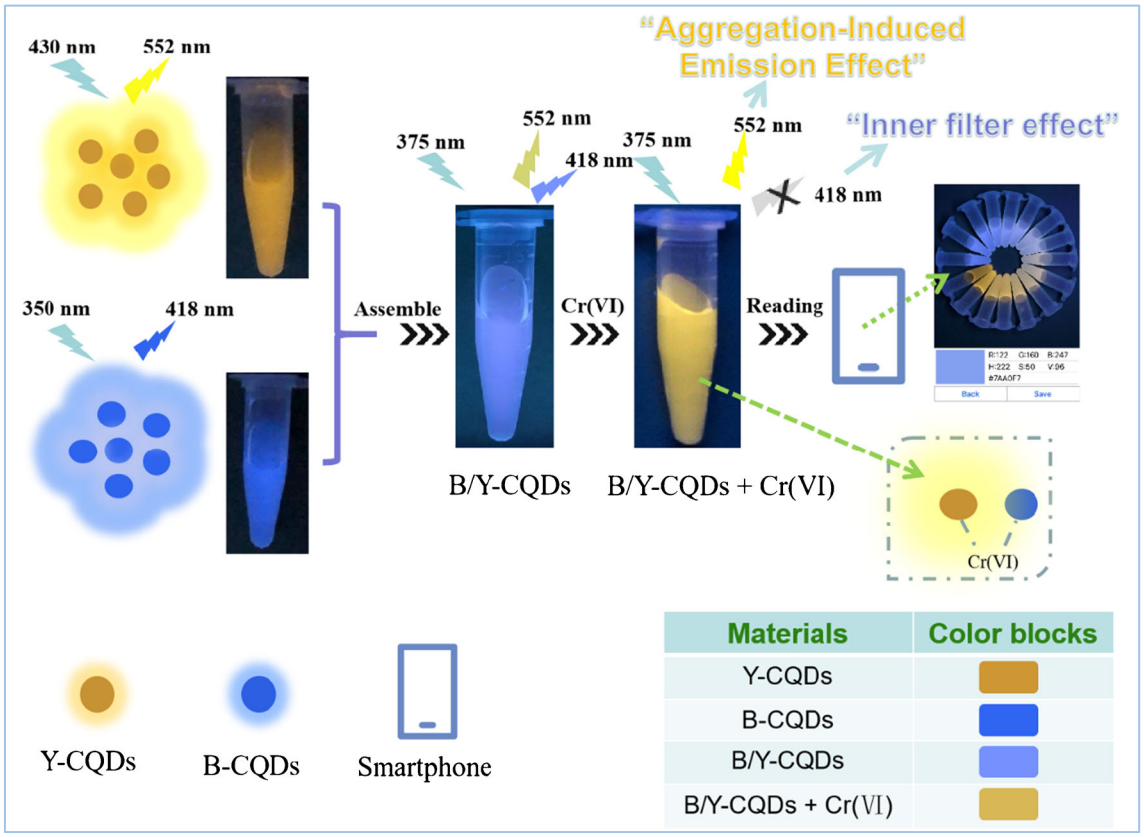

Scheme 1 The principle of exploring the B/Y-CQD fluorescence nanoprobe for Cr(VI) determination and the colour blocks of Y-CQDs, B-CQDs, and B/Y-CQDs (the ratio of B/Y-CQDs was 1:6).

attributed to the n-π* transition of C-O and C=O belonging to the carboxylic groups in B-CQDs. The spectrum of B/Y-CQDs exhibited clear visible absorption bands at 349 nm and 418 nm corresponding to B-CQDs and Y-CQDs.

The fluorescence of the B/Y-CQDs

In this paper, the fluorescent properties of the B/Y-CQDs for the determination of Cr(VI), as well as those of the single B-CQDs and single Y-CQDs are exhibited in Fig. 3a. The ratiometric nanoprobe has two emission peaks compared to single CQDs. Y-CQDs emitted yellow fluorescence with a maximum emission peak of 552 nm under a 430 nm excitation, and the maximum emission wavelength of B-CQDs was 418 nm with high blue fluorescence under a 350 nm excitation (Fig. S2). The two CQDs both possess independent emission peaks accompanied by changing excitation wavelengths, which are attributed to the raw materials used for the synthesis and the temperature [16, 26]. Notably, the characteristic fluorescent peaks of B-CQDs and Y-CQDs can be triggered under 375 nm excitation (Fig. S2). The fluorescence emission peaks of B/Y-CQDs under different excitation wavelengths are exhibited in Fig. S3. The spectra of Y-CQDs and B-CQDs both have clearly integrated peaks under the given excitation wavelengths, while B/Y-CQDs exhibit two integral emission peaks until the excitation wavelength reaches 375 nm. We chose 375 nm as the excitation wavelength for fluorescence spectrophotometer analysis. Moreover, the quantum yields of the as-prepared B-CQDs and Y-CQDs in aqueous solution were 2.58% and 0.61%, respectively, using quinine sulfate as a reference.

Optimization of the experimental conditions

To exclude some possible interferences in real sample analysis and to improve the performance of the B/Y-CQD Cr(VI) detection method, factors including the storage time, light radiation, ionic strength, batches and concentrations of B/Y-CQDs, pH, and incubation time were investigated and optimized. The corresponding results are given in the ESM (Fig. S7–8). The fluorescence response intensity (I_{552}/I_{418}) was used to determine the detection ability of B/Y-CQDs, where I_{552} and I_{418} are the fluorescence intensities of B/Y-CQDs at 418 nm and 552 nm, respectively. The best fluorescence stability conditions and the optimized conditions of B/Y-CQDs in response to Cr(VI) were as follows: (a) for stability of B/Y-CQDs: the best storage time was within 12 h, wherein the B/Y-CQDs could remain constant for 60 min under ultraviolet irradiation (λ_{ex} = 365 nm); (b) optimal ionic strength: 0 M of NaCl was the optimal ionic strength due to its slight impact on

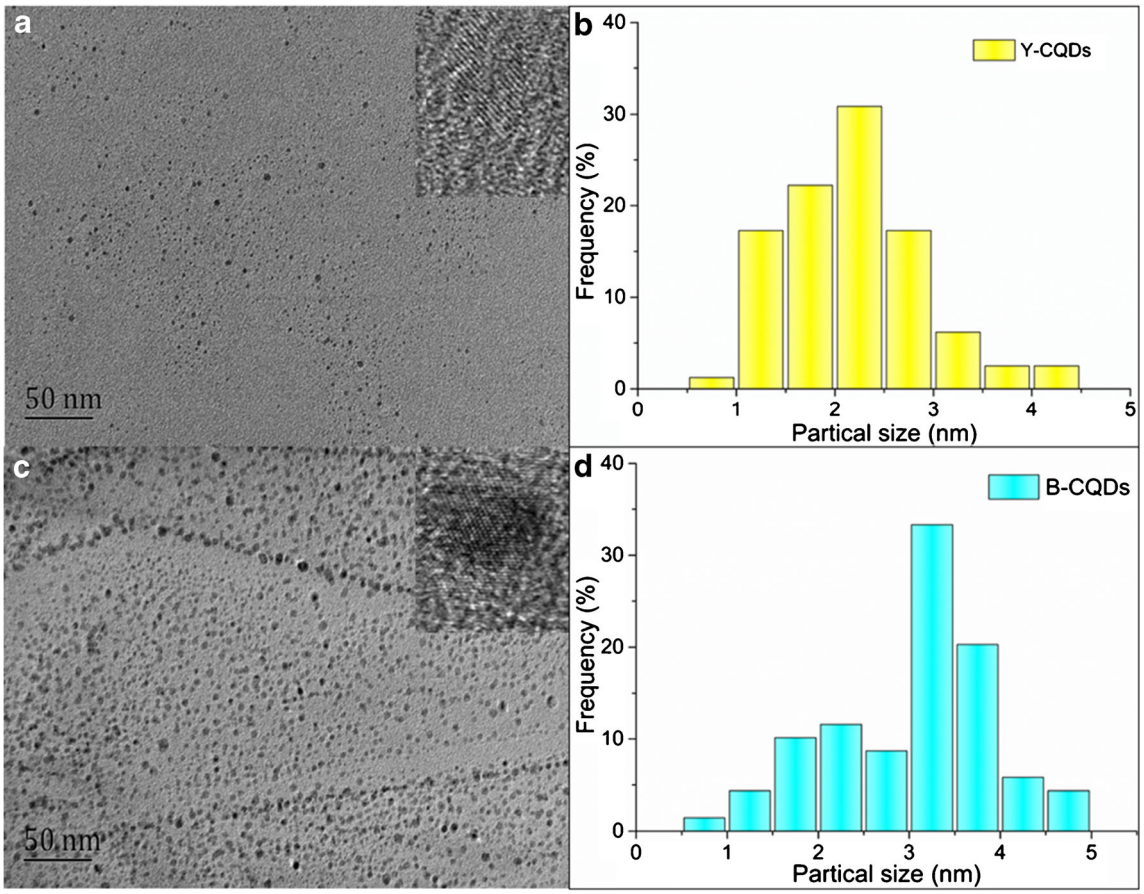

Fig. 1 **a** and **c** TEM images of Y-CQDs and B-CQDs, where the insets in the TEM images show the crystallinity of Y-CQDs and B-CQDs. **b** and **d** Size distributions of the as-synthesized Y-CQDs and B-CQDs. (The concentrations of B-CQDs and Y-CQDs were 22.6 μg/L and 43.2 μg/L, respectively)

B/Y-CQDs; the construction of B/Y-CQDs was repeatable when comparing various batches of B/Y-CQDs; (c) the optimal concentration of B/Y-CQDs: the concentrations of B-CQDs and Y-CQDs were 22.6 and 43.2 μg L^{-1}, respectively; and (d) the best pH value: pH = 7 was selected as the optimal pH. A 15-min incubation time of B/Y-CQDs with Cr(VI) was also evaluated. As shown in Fig. S8b, a stable fluorescence response intensity was obtained within a reaction time of no more than 10 min, indicating that the response time was rapid.

Additionally, the ratio of B-CQDs to Y-CQDs were optimized. B-CQDs and Y-CQDs were mixed in proportions of 2:1, 1:2, 1:4, 1:6, 1:8 and 1:10 to investigate the optimum

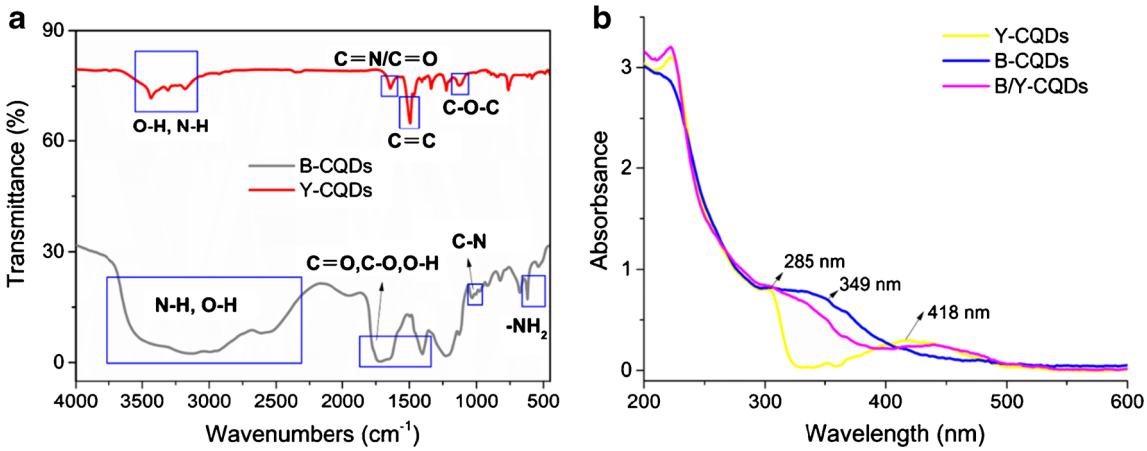

Fig. 2 **a** The FTIR spectrum of Y-CQDs and B-CQDs. **b** UV-Vis absorption spectra of B-CQDs, Y-CQDs and B/Y-CQDs. The concentrations of B-CQDs and Y-CQDs were 22.6 μg/L and 43.2 μg/L, respectively. The ratio of B/Y-CQDs was 1:6

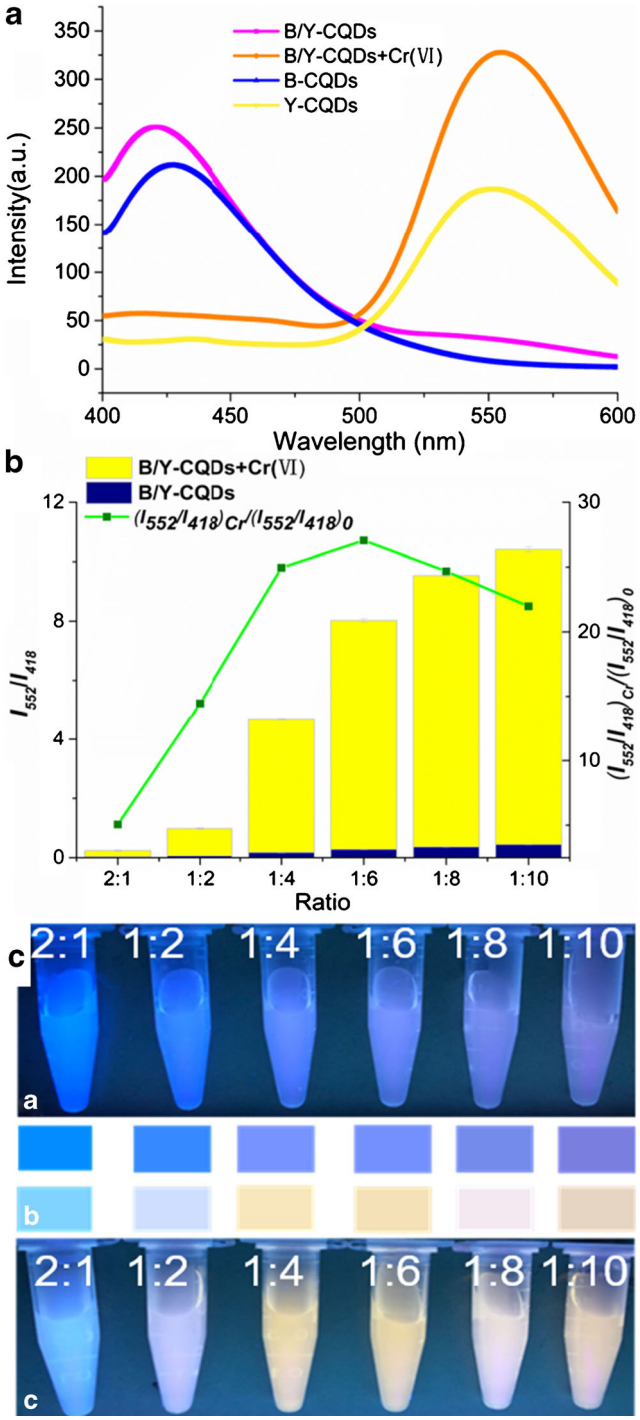

Fig. 3 **a** Fluorescence emission plots of Y-CQDs, B-CQDs, B/Y-CQDs and B/Y-CQDs with Cr(VI). **b** The change in fluorescence intensity of B/Y-CQDs at 418.2 nm and 552.0 nm with and without the addition of Cr(VI) and the ratio values of adding Cr(VI) (I_{Cr}) to no Cr(VI) (I_0) at different compositional proportions (λ_{ex} = 375 nm). **c** Digital photograph of the B/Y-CQDs at different ratios of B-CQDs and Y-CQDs under 365 nm excitation in the absence (a) or presence of C(VI) (c), and (b) their colour blocks. The concentration of Cr(VI) was 167 μM

fluorescence response for Cr(VI) determination (Fig. 3). The proportion of the B/Y-CQDs for the best fluorescent colour was optimized, and the processes displayed apparent colour changes under UV light excitation (365 nm). As displayed in Fig. 3d, the blue emission belonging to B/Y-CQDs was changed to violet upon the addition of Y-CQDs at different proportions. When the ratio of B/Y-CQDs was 1:6, the B/Y-CQDs exhibited two emission peaks at 418 nm and 552 nm under a single wavelength excitation (λ_{ex} = 375 nm) and showed apparent violet fluorescent light under 365 nm UV light. The changes in emission intensities and fluorescence colours were recorded as the B/Y-CQD nanoprobe was added to the target solution. The change in fluorescence intensity (I_{555}/I_{418}) was represented by the results of this intensity ratio before and after adding Cr(VI). The change in fluorescence intensity was the most notable when B-CQDs were mixed with Y-CQDs at a proportion of 1:6 (Fig. 3**b**). Moreover, the colour of the nanoprobe at different ratios is shown in Fig. 3c, and the colour changed to bright yellow when the ratio was 1:6. In summary, we chose a ratio of 1:6 to prepare the B/Y-CQDs.

The detection principle of B/Y-CQDs

The fluorescence interaction of the raw fluorescent materials is discussed to explore the detection principle of the dual-emission B/Y-CQDs. When B-CQDs were mixed with Y-CQDs at a proportion of 1:6, B/Y-CQDs showed a decreased fluorescence peak at 418 nm and an increased fluorescence peak at 552 nm in the presence of Cr(VI). Finally, the peak at 418 nm disappeared, but a strong emission peak was formed at 552 nm because enough Y-CQDs were involved in the enhanced reaction. The B/Y-CQD nanoprobe could quickly and accurately identify Cr(VI) at this ratio. To discuss the phenomenon that occurs when applying the B/Y-CQD nanoprobe for Cr(VI) detection, the fluorescent interaction of each raw fluorescent material of the B/Y-CQD nanoprobe with Cr(VI) should be studied. The result revealed that the fluorescence intensity of single B-CQDs and B-CQDs in B/Y-CQDs gently decreased with an increasing Cr(VI) concentration (Fig. 5a, S5b, S5d). According to previous reports, the fluorescence extinction of fluorescent nanomaterials was caused by Cr(VI) through the IFE [16, 27, 28]. As indicated in Fig. 4a, the ultraviolet absorbance of Cr(VI) could overlap with the fluorescence emission peak of B-CQDs in B/Y-CQDs within the range of 400–500 nm; thus, there is a possible IFE among B-CQDs and Cr(VI). Further, the fluorescence lifetime was used to explore the fluorescence quenching mechanism considering the above phenomenon. The IFE is part of the static quenching mechanism with insignificant variations in the fluorescence lifetime [29, 30]. Fig. S4 shows that the fluorescence decay curve of B/Y-CQDs remained unchanged when Cr(VI) was added, which indicates that a statistical quenching process occurred between B/Y-CQDs and Cr(VI) with the formation of a nonfluorescent complex or compound.

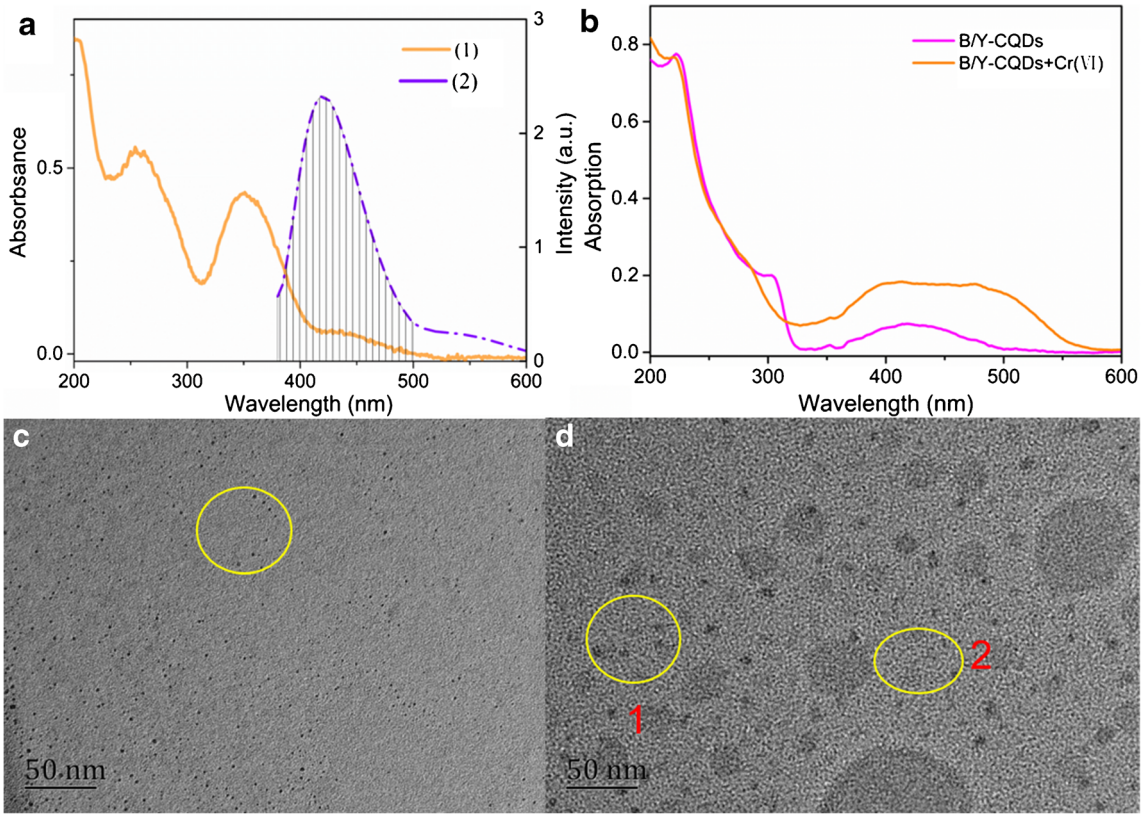

Fig. 4 **a** (1) Absorbance of Cr(VI) and (2) fluorescence emission of B/Y-CQDs under 360 nm excitation. **b** Absorption spectra of B/Y-CQDs in the absence or presence of Cr(VI). **c** Low-resolution TEM image of the B/Y-CQDs. **d** Low-resolution TEM image of the B/Y-CQDs after adding Cr(VI). **1** Aggregated Y-CQDs and **2** B-CQDs. The ratio of B/Y-CQDs was 1:6, and the concentration of Cr(VI) was 167 μM

Therefore, there is evidence that the IFE is the mechanism of fluorescence quenching between the nanoprobe and analyte.

Next, the phenomenon of Y-CQD in B/Y-CQD fluorescence enhancement is worth further discussion. The fluorescence of single Y-CQDs and Y-CQDs in B/Y-CQDs gradually increased with increasing Cr(VI) concentration (Fig. 5a, S5a, S5c). The TEM images of the Y-CQDs, B-CQDs and B/Y-CQDs confirmed the shortened distance between Y-CQD particles after adding Cr(VI), as they combined and aggregated into larger particles, while Cr(VI) had barely effect on B-CQDs (Fig. 4c, d and S6). It can be expected that Cr(VI) can induce aggregation between Y-CQD particles via interactions with the pyrrolic N on the surface of Y-CQDs. In aggregates, intramolecular motions are restricted, and the fluorescence intensity is significantly enhanced [31, 32]. The interaction between Cr(VI) and B/Y-CQDs was explored by determining the absorbance of the B/Y-CQDs. The absorbance peaks of B/Y-CQDs in response to the presence of Cr(VI) are shown in Fig. 4b. The results revealed that an increase in the absorption peak of B/Y-CQDs over the longer wavelength range (350–550 nm) can be observed upon the addition of Cr(VI). The increasing absorbance is likely caused by the aggregation of particles that can both absorb and scatter the incidence light source. These results support the aggregation of B/Y-CQDs in the presence of Cr(VI). With the occurrence of aggregation in a 167 μM Cr(VI) solution, the lifetime of B/Y-CQDs increased from 2.04 ns to 2.51 ns (Table 1), which means that the nonradiative transition was suppressed with the increased radiative transition. The quantum yield of B/Y-CQDs increased from 2.38% to 3.28%, which represented photoluminescence enhancement (Table 1).

Cr(VI) could cause separate fluorescence changes in single B-CQDs and single Y-CQDs because of the independent response to Cr(VI), and this fluorescence variation was sought after in the mixed B/Y-CQDs. Thus, B-CQDs and Y-CQDs could simply be mixed together to form a fluorescence nanoprobe with multiple ratios based on the synchronized responses of both CQDs to Cr(VI). The nanoprobe achieved enhanced selectivity due to the ratiometric fluorescence and colour change with B/Y-CQDs; thus, we chose B/Y-CQDs for further detection studies.

The sensitivity of the B/Y-CQDs to Cr(VI)

To determine the sensing performance of the B/Y-CQD nanoprobe for Cr(VI), different concentrations of Cr(VI) samples (0–1667 μM) were exposed to the B/Y-CQDs separately, and all fluorescence spectra were obtained. As displayed in

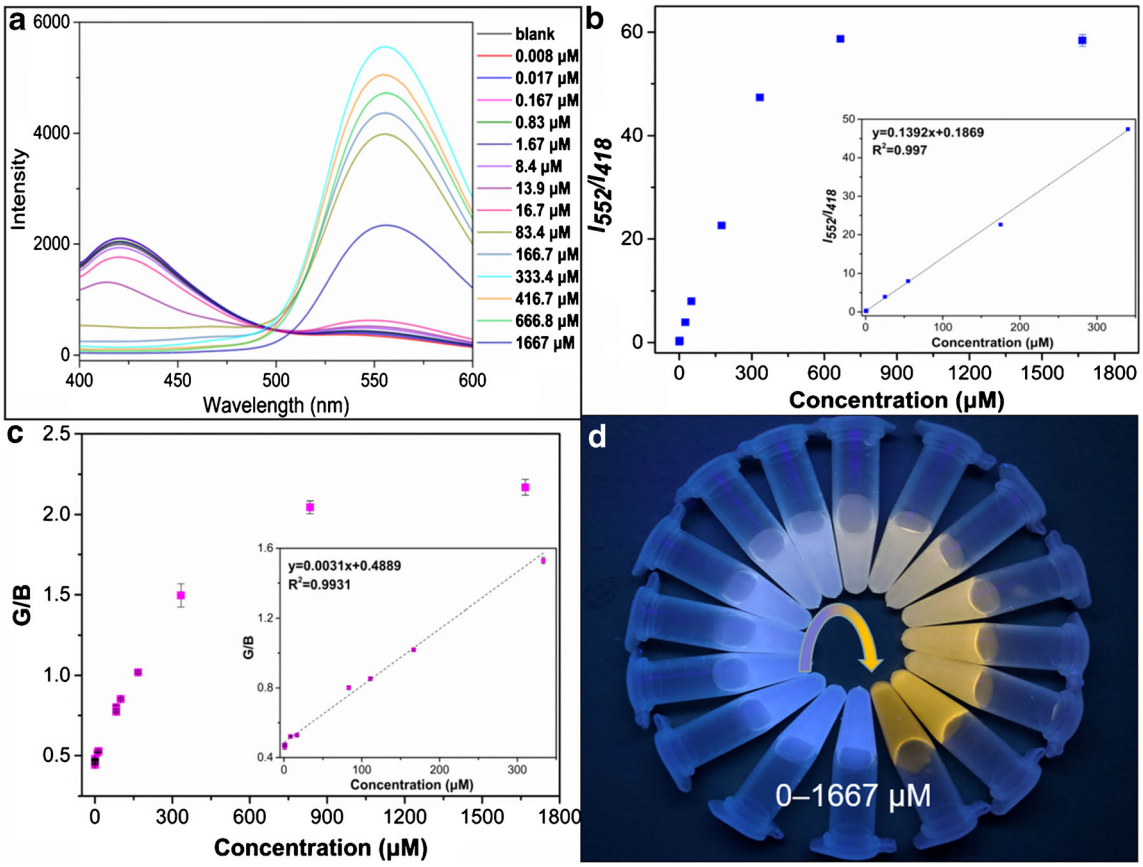

Fig. 5 **a** Fluorescence spectra of B/Y-CQDs in the presence of increasing concentrations of Cr(VI) (0–1667 μM). **b** Plot of the fluorescence intensity ratio (I_{552}/I_{418}) for various concentrations of Cr(VI) (0–1667 μM). Inset: The linear range of I_{552}/I_{418} at different concentrations (0.3–333.2 μM). **c** Plot of the visualization analysis (G/B) under different concentrations (0–1667 μM). Inset: The linear range of the visualization analysis under different concentrations (0.8–333.2 μM). **d** Fluorescence images under UV light in the presence of different Cr(VI) samples. The ratio of B/Y-CQDs was 1:6

Fig. 5a, the obvious decrease in the B/Y-CQDs emission intensity occurred at 418 nm with increased concentrations of Cr(VI). Moreover, there was an equally radical change at 552 nm as the concentration of Cr(VI) increased from 0 μM to 1667 μM. The fluorescence intensities of CQDs could be influenced by Cr(VI), in which the yellow emission was enhanced and reinforced the fluorescent colour change for detection. The relative ratio of the fluorescence intensity of the dual-emission B/Y-CQDs was selected to evaluate the nanoprobe sensitivity. The fluorescence intensity ratio (I_{552}/I_{418}) exhibited good linearity with Cr(VI) concentrations from 0.3 to 333.2 μM (Fig. 5b). The regression equation can be expressed as $I_{552}/I_{418} = 0.1392x + 0.1869$, where x is the Cr(VI) concentration in moles per litre and the correlation coefficient is 0.997, which shows strong linearity. The limit of detection (LOD) was estimated to be 0.04 μM ($S/N = 3$).

Further, an on-site fluorescent measurement was recorded by the smartphone, and the RGB values were obtained. This method was used to obtain fluorescence standard images, including RGB values, under different Cr(VI) concentrations (0–1667 μM) (Fig. 5d). The fluorescence colour of B/Y-CQDs changed regularly with increasing Cr(VI), as distinguished by the naked eye. This method could be used for the visual detection of Cr(VI) based on fluorescence colour changes. The ratio that takes into account the G values and B values of the RGB values, which can display the fluorescent colour change, exhibited linear dependence in the range of 0.8–333.2 μM with an LOD of 0.55 μM (Fig. 5c). The regression equation can be expressed as $G/B = 0.0031x + 0.4889$, where x is the Cr(VI) concentration in moles per litre and with a correlation coefficient of 0.9935. The fluorescent measurement expanded the detection range simply and conveniently. From the results described above, the limits of detection of the two types of detection modes were both lower than the limitation of 0.05 μg ml^{-1} (~1 μM) for drinking water, which was recommended by the World Health Organization [33].

The selectivity of B/Y-CQD nanoprobes

The complexity of real samples presents an enormous challenge for B/Y-CQDs detection of Cr(VI) not only in terms of sensitivity but also, more fundamentally, in terms of specificity.

Table 1 Fluorescence lifetimes and quantum yields of B-CQDs, Y-CQDs and B/Y-CQDs. The ratio of B/Y-CQDs was 1:6, and the concentration of Cr(VI) was 167 μM.

Nanomaterials	B-CQDs	Y-CQDs	B/Y-CQDs with no Cr(VI)	B/Y-CQDs with Cr(VI)
Fluorescence lifetime τ (ns)	1.87	6.64	2.04	2.51
Quantum yield	2.58%	0.61%	2.38%	3.28%

As a result, we discuss the effect of nontarget interferences on the ratiometric nanoprobe. The interference substances were Ag(I), Cd(II), K(I), Cr(III), Al(III), Ca(II), Co(III), Na(I), Zn(II), Hg(II), Fe(III), Mn(II), Fe(II), Pb(II), Mg(II), Cu(II), tannic acid, β-lactoglobulin, casein and bovine serum albumin (BSA). As exhibited in Fig. 6a and b, many substances did not interfere with the ratio of the fluorescence intensity (I_{552}/I_{418}); only Cr(VI) decreased the emission intensity of B-CQDs and enhanced the emission intensity of Y-CQDs, achieving the dual-fluorescence response mode. Some species exhibited interferences probably because of the occurrence of electron transfer with B-CQDs, and Fe(III) was the main interfering factor because of its paramagnetic properties [34]. Nevertheless, the fluorescence quenching caused by these interference substances was very weak compared with Cr(VI). The as-prepared B/Y-CQDs showed a highly selective response to Cr(VI) as a ratiometric nanoprobe.

Determination of Cr(VI) in real samples

Chromium is considered a serious environmental pollutant due to its wide industrial use. It easily contaminates water, soil and plants, including herbs and foodstuff, and then accumulates in the food chain, thus posing potential threats due to the mobile and toxic properties of chromium [35]. Therefore, we measured Cr(VI) in tap water and two food samples consisting of milk and green tea to validate the practicability of the B/Y-CQDs. The real samples were diluted with deionized water for

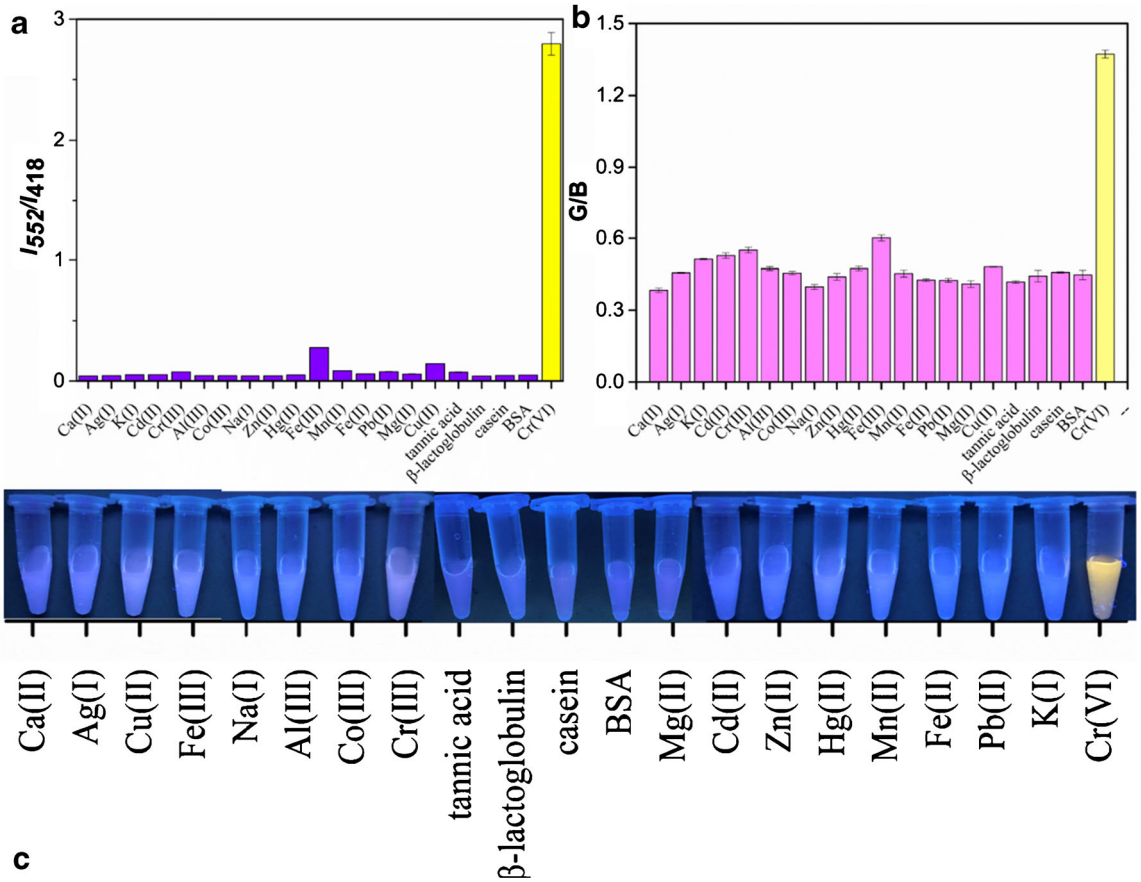

Fig. 6 **a** The fluorescence intensity of the B/Y-CQD aqueous solution in the presence of 330 μM of different metal ion interferents and the target at 167 μM (λ_{ex} = 375 nm). **b** The RGB relative ratio values of the fluorescent images in the presence of different analytes. **c** Corresponding photograph under UV light. The ratio of B/Y-CQDs was 1:6

Table 2. Comparison of the determination methods for Cr(VI)

Nanoprobe	LOD* (μM)	Recoveries (%)	Real samples	Linear range (μM)	Ref.
Cobalt-doped carbondots	1.17	83.69-106.96	tap water/fish	5 -125	[37]
Silicon quantum dots	0.16	97.2~108.5	lotus seeds	0.5-500	[38]
Graphene quantum dots	0.0037	95.4 - 104.8	water samples	0.05-500	[39]
B/Y-CQDs	0.04 μM; 0.55 μM	81.6-107.7	tap water/food samples	0.3-333.2; 0.8-333.2	This work

* LOD: limit of detection

further detection. In a typical experiment, 250 μL of B/Y-CQDs was mixed with 250 μL of the diluted real samples and vortexed for 30 s. The mixture was equilibrated for a few minutes under ambient conditions and studied with the prepared ratiometric method. The standard addition method with Cr(VI) was applied because no Cr(VI) was detected in the water samples. The maximum allowed concentration in water is 0.05 mg L^{-1} (~1 μM), so we chose relatively low concentrations (2, 6 and 12 μM) for the spiked concentrations of the analyte [36]. The pretreated samples were mixed with Cr(VI) at various concentrations. After the samples reached equilibrium, we recorded the fluorescence intensity ratio (I_{552}/I_{418}) of the samples and the RGB values of the fluorescence images. The results in Table S1 imply that these sample recoveries ranged from 84.6–103.3% with a relative standard deviation (RSD) within 4.4%. Moreover, on-site fluorescent measurements were also performed. The analytical results of real samples showed that the on-site method had sufficient precision and recoveries in the range of 81.6–107.7% with an RSD below 2.3% under a high concentration of Cr(VI) (Table S2). The test results of real samples verified that the ratiometric B/Y-CQDs had good practicability for monitoring Cr(VI) in practical systems. Finally, the green tea samples had a weaker response to Cr(VI) than the other samples, which was mainly due to the reductive interferent (ascorbic acid) that can reduce Cr(VI) to Cr(III), after which the original fluorescence signal was recovered [16]. Based on the actual sample application, the effect of reductive interferent on the reversibility of the B/Y-CQDs for Cr(VI) determination is worth further explored in the future. Finally, compared with the previous literature reports listed in Table 2, we find that all these chemosensors are capable of detecting Cr(VI); however, they still suffer from a tedious synthesis procedure. The B/Y-CQDs presented in this work has good performance in terms of the LOD and detection concentration range without the use of tedious methods. Equally notable is that the need for UV light makes the probe prone to interference by biomatter. Marine water, wastewaters, etc. always display strong background UV absorption and fluorescence. The UV light used for fluorescence excitation is screened by UV absorbers, which weakens the signal. This problem, in turn, will be the research focus for fluorescence visualization applications.

Conclusion

A simple and visualization-enabled ratiometric fluorescent detection system for Cr(VI) was demonstrated based on a dual-emission fluorescent nanoprobe. The introduction of Cr(VI) led to the fluorescence quenching of B-CQDs due to the IFE, while Cr(VI) resulted in the fluorescence enhancement of Y-CQDs owing to the AIEE. The nanoprobe is worth further research and development in terms of its stability and practicability for actual sample measurements. As a result, this method was also applied for the analysis of Cr(VI) in real samples with satisfactory results.

Supplementary Information The online version contains supplementary material available at https://doi.org/10.1007/s00604-021-04747-8.

Acknowledgements This work was supported by the Open Project Program of the State Key Laboratory of Food Nutrition and Safety, Tianjin University of Science & Technology (No. SKLFNS-KF-201908), and the National Natural Science Foundation of China (No. 21806083).

Author contributions **Yao Chixuan**: Conceptualization, Methodology, Investigation, Writing - Original Draft. **Liu Qingrun**: Data Curation, Validation. Zhao Ning: Visualization. **Liu Jing-Min**: Writing-Reviewing and Editing. **Fang Guozhen**: Project administration. **Wang Shuo**: Supervision, Funding acquisition.

Declarations

Conflict of interest The authors declare that they have no conflicts of interest.

References

1. Tan X, Wang X, Hao A, Liu Y, Wang X, Chu T, Jiang L, Yang Y, Ming D (2020) Aptamer-based ratiometric fluorescent nanoprobe for specific and visual detection of zearalenone. Microchem J 157: 104943. https://doi.org/10.1016/j.microc.2020.104943
2. Wang B, Liang Z, Tan H, Duan W, Luo M (2020) Red-emission carbon dots-quercetin systems as ratiometric fluorescent nanoprobes towards Zn^{2+} and adenosine triphosphate. Microchim Acta 187(6):345. https://doi.org/10.1007/s00604-020-04316-5
3. Tan H, Wu X, Weng Y, Lu Y, Huang Z-Z (2020) Self-assembled FRET Nanoprobe with metal-organic framework as a scaffold for

Ratiometric detection of Hypochlorous acid. Anal Chem 92(4): 3447–3454. https://doi.org/10.1021/acs.analchem.9b05565
4. Wang Y-Q, Zhao T, He X-W, Li W-Y, Zhang Y-K (2014) A novel core-satellite CdTe/silica/au NCs hybrid sphere as dual-emission ratiometric fluorescent probe for Cu^{2+}. Biosens Bioelectron 51: 40–46. https://doi.org/10.1016/j.bios.2013.07.028
5. Doussineau T, Schulz A, Lapresta-Fernandez A, Moro A, Körsten S, Trupp S, Mohr GJ (2010) On the Design of Fluorescent Ratiometric Nanosensors. Chem Eur J 16(34):10290–10299. https://doi.org/10.1002/chem.201000829
6. Li P, Xie T, Fan N, Li K, Tang B (2011) Ratiometric fluorescence imaging for distinguishing chloride concentration between normal and ischemic ventricular myocytes. Chemical communications (Cambridge, England) 48:2077-2079. https://doi.org/10.1039/c1cc15258k
7. Yu L, Zhang L, Ren G, Li S, Zhu B, Chai F, Qu F, Wang C, Su Z (2018) Multicolorful fluorescent-nanoprobe composed of au nanocluster and carbon dots for colorimetric and fluorescent sensing Hg^{2+} and Cr^{6+}. Sensors Actuators B Chem 262:678–686. https://doi.org/10.1016/j.snb.2018.01.192
8. Liu W, Wang X, Wang Y, Li J, Shen D, Kang Q, Chen L (2018) Ratiometric fluorescence sensor based on dithiothreitol modified carbon dots-gold nanoclusters for the sensitive detection of mercury ions in water samples. Sensors Actuators B Chem 262:810–817. https://doi.org/10.1016/j.snb.2018.01.222
9. Barakat MA (2011) New trends in removing heavy metals from industrial wastewater. Arab J Chem 4(4):361–377. https://doi.org/10.1016/j.arabjc.2010.07.019
10. Das A, Mishra S (2009) Hexavalent chromium (VI): environment pollutant and health hazard. J Environ Res Dev 2:386–392
11. Das R, Bandyopadhyay R, Pramanik P (2018) Carbon quantum dots from natural resource: a review. Materials Today Chemistry 8:96–109. https://doi.org/10.1016/j.mtchem.2018.03.003
12. Sharma P, Rajput P, Thakur A, Kim K-H, Kumar P (2019) Recent advances in carbon quantum dot-based sensing of heavy metals in water. TrAC Trends Anal Chem 114:171–195. https://doi.org/10.1016/j.trac.2019.03.003
13. Xu S, Zhang F, Xu L, Liu X, Ma P, Sun Y, Wang X, Song D (2018) A fluorescence resonance energy transfer biosensor based on carbon dots and gold nanoparticles for the detection of trypsin. Sensors Actuators B Chem 273:1015–1021. https://doi.org/10.1016/j.snb.2018.07.023
14. Zhang S, Lin B, Yu Y, Cao Y, Guo M, Shui L (2018) A ratiometric nanoprobe based on silver nanoclusters and carbon dots for the fluorescent detection of biothiols. Spectrochim Acta A Mol Biomol Spectrosc 195:230–235. https://doi.org/10.1016/j.saa.2018.01.078
15. Wang L, Cao H-X, He Y-S, Pan C-G, Sun T-K, Zhang X-Y, Wang C-Y, Liang G-X (2019) Facile preparation of amino-carbon dots/gold nanoclusters FRET ratiometric fluorescent probe for sensing of Pb^{2+}/Cu^{2+}. Sensors Actuators B Chem 282:78–84. https://doi.org/10.1016/j.snb.2018.11.058
16. Vaz R, Bettini J, Junior J, Lima E, Botero W, Carinhanha Caldas Santos J, Schiavon M (2017) High luminescent carbon dots as an eco-friendly fluorescence sensor for Cr(VI) determination in water and soil samples. J Photochem Photobiol A Chem 346:502–511. https://doi.org/10.1016/j.jphotochem.2017.06.047
17. Zhao J, Li F, Zhang S, An Y, Sun S (2019) Preparation of N-doped yellow carbon dots and N, P co-doped red carbon dots for bioimaging and photodynamic therapy of tumors. New J Chem 43(16):6332–6342. https://doi.org/10.1039/C8NJ06351F
18. Zhang R, Chen W (2014) Nitrogen-doped carbon quantum dots: facile synthesis and application as a "turn-off" fluorescent probe for detection of Hg^{2+} ions. Biosens Bioelectron 55:83–90. https://doi.org/10.1016/j.bios.2013.11.074
19. Campos BB, Oliva MM, Contreras-Cáceres R, Rodriguez-Castellón E, Jiménez-Jiménez J, da Silva JCGE, Algarra M (2016) Carbon dots on based folic acid coated with PAMAM dendrimer as platform for Pt(IV) detection. J Colloid Interface Sci 465: 165–173. https://doi.org/10.1016/j.jcis.2015.11.059
20. Song Y, Zhu C, Song J, Li H, Du D, Lin Y (2017) Drug-derived bright and color-tunable N-doped carbon dots for cell imaging and sensitive detection of Fe^{3+} in living cells. ACS Appl Mater Interfaces 9(8):7399–7405. https://doi.org/10.1021/acsami.6b13954
21. Song L, Cui Y, Zhang C, Hu Z, Liu X (2016) Microwave-assisted facile synthesis of yellow fluorescent carbon dots from o-phenylenediamine for cell imaging and sensitive detection of Fe^{3+} and H_2O_2. RSC Adv 6(21):17704–17712. https://doi.org/10.1039/C6RA02554D
22. Vedamalai M, Periasamy AP, Wang C-W, Tseng Y-T, Ho L-C, Shih C-C, Chang H-T (2014) Carbon nanodots prepared from o-phenylenediamine for sensing of Cu^{2+} ions in cells. Nanoscale 6(21):13119–13125. https://doi.org/10.1039/C4NR03213F
23. Shieh Y-T, Chen J-Y, Twu Y-K, Chen W-J (2012) The effect of pH and ionic strength on the dispersion of carbon nanotubes in poly(-acrylic acid) solutions. Polym Int 61(4):554–559. https://doi.org/10.1002/pi.3203
24. Ju J, Zhang R, He S, Chen W (2014) Nitrogen-doped graphene quantum dots-based fluorescent probe for the sensitive turn-on detection of glutathione and its cellular imaging. RSC Adv 4(94): 52583–52589. https://doi.org/10.1039/C4RA10601F
25. Zhang Y, Cui P, Zhang F, Feng X, Wang Y, Yang Y, Liu X (2016) Fluorescent probes for "off–on" highly sensitive detection of Hg^{2+} and L-cysteine based on nitrogen-doped carbon dots. Talanta 152: 288–300. https://doi.org/10.1016/j.talanta.2016.02.018
26. Zhuo Y, Miao H, Zhong D, Zhu S, Yang X (2015) One-step synthesis of high quantum-yield and excitation-independent emission carbon dots for cell imaging. Mater Lett 139:197–200. https://doi.org/10.1016/j.matlet.2014.10.048
27. Kim H, Lee B-I, Byeon S-H (2015) The inner filter effect of Cr(vi) on Tb-doped layered rare earth hydroxychlorides: new fluorescent adsorbents for the simple detection of Cr(vi). Chem Commun 51(4):725–728. https://doi.org/10.1039/C4CC08543D
28. Zhang D, Dong Z, Jiang X, Feng M, Li W, Gao G (2013) A proof-of-concept fluorescent strategy for highly selective detection of Cr(vi) based on inner filter effect using a hydrophilic ionic chemosensor. Anal Methods 5(7):1669–1675. https://doi.org/10.1039/C3AY26555B
29. Sun J, Zhao J, Wang L, Li H, Yang F, Yang X (2018) Inner filter effect-based sensor for horseradish peroxidase and its application to fluorescence immunoassay. ACS Sensors 3(1):183–190. https://doi.org/10.1021/acssensors.7b00830
30. Gu W, Pei X, Cheng Y, Zhang C, Zhang J, Yan Y, Ding C, Xian Y (2017) Black phosphorus quantum dots as the Ratiometric fluorescence probe for trace mercury ion detection based on inner filter effect. ACS Sensors 2(4):576–582. https://doi.org/10.1021/acssensors.7b00102
31. Jia X, Li J, Wang E (2013) Cu Nanoclusters with aggregation induced emission enhancement. Small 9(22):3873–3879. https://doi.org/10.1002/smll.201300896
32. Park S, Seo J, Kim SH, Park SY (2008) Tetraphenylimidazole-based excited-state Intramolecular proton-transfer molecules for highly efficient blue electroluminescence. Adv Funct Mater 18(5): 726–731. https://doi.org/10.1002/adfm.200700827
33. Jain CK, Bandyopadhyay A, Bhadra A (2010) Assessment of ground water quality for drinking purpose, district Nainital, Uttarakhand, India. Environ Monit Assess 166(1):663–676. https://doi.org/10.1007/s10661-009-1031-5
34. Chuanxi W, Jiang K, Xu Z, Lin H, Zhang C (2016) Glutathione modified carbon-dots: from aggregation-induced emission

enhancement property to "turn-on" sensing of temperature/Fe^{3+} ions in cells. Inorg Chem Front 3:514–522. https://doi.org/10.1039/C5QI00273G

35. Wang H, Jiang Y, Tian C, Pan R, Dang F, Feng J, Li M, Zhang Y, Li H, Man C (2018) Determination of the transfer of lead and chromium from feed to raw milk in Holstein cows. Food Additives & Contaminants: Part A 35(10):1990–1999. https://doi.org/10.1080/19440049.2018.1496279
36. Organization W (2011) Guidelines for drinking-water quality
37. Zhang H, Wang Y, Xiao S, Wang H, Wang J-H, Feng L (2016) Rapid detection of Cr(VI) ions based on cobalt(II)-doped carbon dots. Biosens Bioelectron 87:46–52. https://doi.org/10.1016/j.bios.2016.08.010
38. Xu W, Yu L, Xu H, Zhang S, Xu W, Lin Y, Zhu X (2019) Water-dispersed silicon quantum dots for on-off-on fluorometric determination of chromium(VI) and ascorbic acid. Microchim Acta 186(10):673. https://doi.org/10.1007/s00604-019-3751-8
39. Huang S, Qiu H, Zhu F, Lu S, Xiao Q (2015) Graphene quantum dots as on-off-on fluorescent probes for chromium(VI) and ascorbic acid. Microchim Acta 182(9):1723–1731. https://doi.org/10.1007/s00604-015-1508-6